



Glass Segmentation with Fusion of Learned and General Visual Features

Risto Ojala¹, Tristan Ellison², and Mo Chen²

¹ Aalto University, Espoo, Finland (risto.ojala@aalto.fi)

² Simon Fraser University, Burnaby, Canada

Abstract. Glass surface segmentation from RGB images is a challenging task, since glass as a transparent material distinctly lacks visual characteristics. However, glass segmentation is critical for scene understanding and robotics, as transparent glass surfaces must be identified as solid material. This paper presents a novel architecture for glass segmentation, deploying a dual-backbone producing general visual features as well as task-specific learned visual features. General visual features are produced by a frozen DINOv3 vision foundation model, and the task-specific features are generated with a Swin model trained in a supervised manner. Resulting multi-scale feature representations are downsampled with residual Squeeze-and-Excitation Channel Reduction, and fed into a Mask2Former Decoder, producing the final segmentation masks. The architecture was evaluated on four commonly used glass segmentation datasets, achieving state-of-the-art results on several accuracy metrics. The model also has a competitive inference speed compared to the previous state-of-the-art method, and surpasses it when using a lighter DINOv3 backbone variant. The implementation source code and model weights are available at: <https://github.com/ojalar/lgnet>.

Keywords: Glass segmentation · Semantic segmentation · Foundation models

1 Introduction

Glass surface segmentation has been a widely studied problem in the image processing community [12, 16]. Robotic perception and scene understanding applications are reliant on accurate detection of glass surfaces. Due to glass being a transparent material, sensors such as cameras and LiDAR have difficulty correctly registering these surfaces as solid material. Nevertheless, correctly registering these solid surfaces is critical for obstacle avoidance and navigation of mobile robots.

Many modalities have been experimented with for glass segmentation, such as LiDAR [27], RGB-D images [11], and infrared images combined with RGB images [9]. However, glass segmentation from RGB images has remained the most widely studied modality due to its broad applicability, as monocular RGB cameras are some of the cheapest and most commonly used sensors. The fundamental

problem of glass segmentation from RGB images lies in the fact that the visual appearance of a glass surface can highly or completely resemble the appearance of the scene behind it. Additionally, reflections can majorly affect the appearance of a glass surface. Since glass surfaces have a complex and at times non-existent visual appearance, successful detection of a glass surface can often be highly dependent on understanding the visual context. Similarly to human intuition, a deep learning model with an advanced semantic understanding and reasoning may correctly predict the existence of a glass surface purely by observing the surrounding scene. Therefore, foundation models offer a prominent direction for expanding the capabilities of glass segmentation.

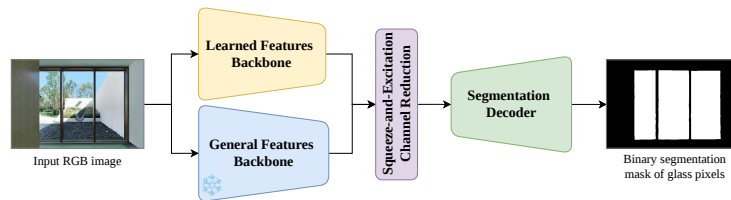


Fig. 1: High-level overview of the proposed L+GNet architecture. A dual-backbone is constructed, which utilizes a Learned Features Backbone for generating task-specific features, and a frozen General Features Backbone for context from a vision foundation model.

This work proposes a novel architecture, L+GNet, for glass segmentation from RGB images, based on a dual-backbone architecture. An overview of the proposed architecture is presented in Fig. 1. The dual-backbone combines task-specific visual features learned in a supervised manner, with general visual features acquired from a foundation model. The intuition behind the architecture is to tap into the vast contextual information of a foundation model, while incorporating features learned directly from relevant data. This design choice ensures that the architecture is highly generalizable, as shown via experiments on four different glass segmentation datasets. For processing the large number of features produced by the dual-backbone, a novel channel reduction strategy is presented, enabling the extraction of relevant information. The resulting feature representation is fed to a decoder module, which produces the final segmentation masks.

The main contributions of this work can be summarized as follows:

- The paper proposes the L+GNet architecture for the glass segmentation task, containing a novel dual-backbone producing both general and task-specific features from input images.
- Squeeze-and-Excitation (SE) Channel Reduction is proposed for effectively fusing the outputs of the dual-backbone.
- Experimental results show that the L+GNet architecture achieves state-of-the-art results on multiple datasets in terms of accuracy, while maintaining a reasonable computational load.

2 Related Work

2.1 Glass Segmentation

Segmenting glass remains a difficult task due to its textureless, transparent and reflective nature. The first deep learning glass segmentation method was proposed in [16]. Since then, many works have contributed by creating new datasets and techniques. Numerous approaches have used primarily convolutional neural networks (CNNs) [6, 12, 16–18, 23, 25, 26]. Most of the architectures deploy different types of channel and spatial attention mechanisms, similar to [22]. A popular segmentation strategy has been the utilization of multi-scale features to extract deeper global context while preserving high-resolution spatial information [6, 12, 17, 25]. Many networks have incorporated mechanisms focused on detecting inherent properties of glass. GSDNet [12] focuses specifically on the visible reflections present on glass surfaces. During training, a pre-trained reflection detection network was used to guide the predictions of the GSDNet framework. VBNet [18] applies a multi-scale segmentation architecture where the low-level features are processed applying visual blurriness blocks in the encoder and the decoder. Visual blurriness was implemented as an average pooling operation, run in parallel with other network layers. As glass itself is difficult to visually detect, the TransLab [25] architecture focuses on specifically identifying the borders of glass surfaces. The architecture includes a dual-decoder architecture, with a specialized head for boundary detection. As an alternative to the more traditional CNNs, transformer models have also been developed for glass segmentation [23, 26].

More recent works have explored the use of frozen backbones and diffusion models in glass segmentation. GlassWizard [10] employs a two-step process using Stable Diffusion 2.0 [19] to extract semantic and contextual priors by using a trainable prompt and freezing the diffusion model. In the second phase of training, the diffusion model is trained while the prompt is frozen. Foundation models have also been used for segmentation, but with limited task-specific data, it becomes challenging to meaningfully fine-tune these large models. Controllable-LPMoE [21] circumvents this by building trainable features around and into a vision foundation model, while also applying different convolutional kernels to extract unique semantic data. As the most recent works, Controllable-LPMoE and GlassWizard hold the latest state-of-the-art accuracies in the glass segmentation task.

Most similar to the architecture proposed in this paper, GlassSemNet [13] utilizes a dual-backbone architecture with a ResNet50 [7] for feature extraction, and a SegFormer [24] to extract semantic information. The semantic backbone performs semantic segmentation on the input images, providing masks for pre-defined classes, such as curtains, blinds, cabinets, and sinks. Proposing their own semantically enriched dataset, GSD-S, the semantic information was proven to be valuable when predicting glass masks. However, the GSD-S dataset is limited to 43 classes, which can limit practical applicability in different environments.

2.2 Recent Advancements in Computer Vision

Vision transformers, ViTs [3] have been shown to excel in computer vision, by processing image patches with a global self-attention mechanism. The Swin Transformer [14] innovated on the basic idea of ViTs by applying window-level attention, with a constant number of patches in each window. Window and patch sizes increase progressively in the network, enabling global attention while scaling linearly with respect to input image size. The network also shifts window boundaries to prevent feature cut-off in the patching process. Transformers are generally the most successful models in a number of computer vision tasks. In segmentation tasks, the Mask2Former [2] decoder has been shown to perform well in a large number of applications.

Vision foundation models have emerged based on the learning capabilities of the vision transformers. These models utilize an extensive self-supervised training process to learn meaningful, generalizable feature representations. DINOv3 [20] is a recent vision foundation model, trained on an immense data pool of approximately 17 billion images. The model provides detailed and general-purpose feature maps. These features can be used for multiple tasks, including depth perception, semantic segmentation, and instance recognition with minimal layers on top of the original network.

2.3 Research Gap

Foundation models have previously been applied for glass segmentation in [21]. This paper proposes a novel strategy for using vision foundation models in glass segmentation. The presented L+GNet model features a novel dual-backbone architecture, which fuses the foundation model output with the output of a separate learned backbone. The dual-backbone architecture has similarities to the model proposed by [13] for glass segmentation. However, the previously proposed dual-backbone architecture utilized an explicitly trained semantic segmentation model for extracting context in the other backbone. The semantic backbone in this previous approach is limited to the classes that it has been taught during training. We propose to apply a foundation model in the dual-backbone, providing general visual features instead of explicitly trained semantic class information. This novel approach offers improved generalizability and richer feature representations compared to simple semantic masks. The design choices of the proposed architecture are proven to provide state-of-the-art results via experiments on multiple datasets.

3 Methods

Given an input RGB image, the analyzed task is to generate a binary segmentation mask correctly classifying each pixel in the image. Each pixel in an image is classified to contain either “glass” or “background”. We propose a novel deep learning architecture, coined L+GNet, for the glass segmentation task. The architecture is trained via supervised learning, using annotated datasets for training the model to distinguish glass in RGB images.

3.1 Model Architecture

The developed model utilises a novel dual-backbone to generate both learned and general features from input images. The dual-backbone consists of a Learned Features Backbone and a General Features Backbone. The intuition behind the dual-backbone is to utilize the vast capabilities of current foundation models, while still learning task-specific features. Features from the dual-backbone are concatenated and fed through residual SE blocks [8], while reducing the number of feature channels. The resulting features are processed into segmentation masks with a Mask2Former Decoder [2]. The architecture of the proposed L+GNet is visualized in Fig. 2, and the building blocks of the architecture are described below.

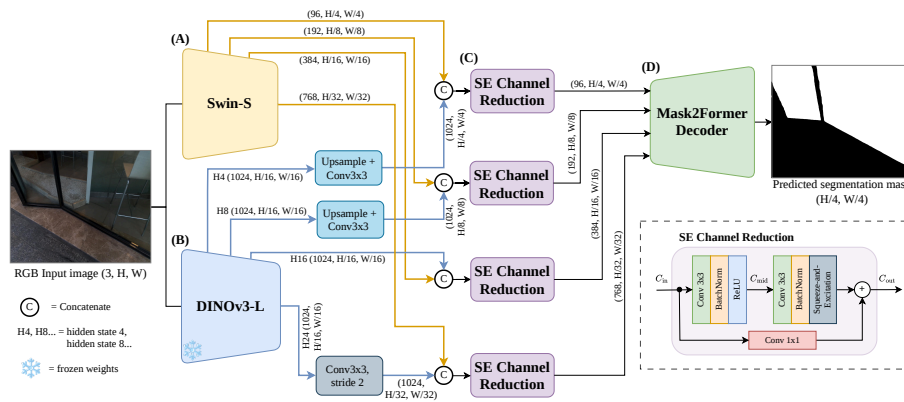


Fig. 2: The proposed L+GNet architecture. Bottom right corner shows the detailed contents of a SE Channel Reduction block. Labels (A)-(D) refer to corresponding sub-sections, which contain detailed descriptions of the specific blocks.

Learned Features Backbone (A) The Learned Features Backbone is incorporated into the architecture to learn relevant, task-specific feature representations from available training data for glass segmentation. A Swin-S transformer model was chosen as the Learned Features Backbone of the L+GNet architecture. As a transformer-based model, Swin-S not only captures local features, but also long-range spatial dependencies through shifted window-based self-attention.

Swin-S produces hierarchical, multi-scale feature representations at sizes of $1/4$, $1/8$, $1/16$ and $1/32$ of the input image dimensions. Higher resolution features are useful for producing high resolution segmentation masks. The higher resolution features are a valuable contribution of the Learned Features Backbone, as the General Features Backbone applied here produces feature maps with a patch size of 16×16 pixels. Large patch sizes are common for foundation

models, as the models are typically based on the ViT-architecture and apply global self-attention mechanisms.

General Features Backbone (B) Foundation models are capable of producing general-purpose feature representations for images based on self-supervised training on vast datasets. The General Features Backbone of the L+GNet architecture applies a foundation model to extract general visual features from the input image. Due to the limited visual information found directly in transparent glass surfaces, the general features offer important global context for the segmentation task.

DINOv3-L was chosen as the foundation model for the General Features Backbone. The weights of the model are frozen in the L+GNet architecture, not being optimized during training. DINOv3-L is used in the General Features Backbone by extracting different hidden states from the model, acquiring feature representations from different stages of processing. The model outputs are the hidden states of the patch embeddings after transformer blocks (6, 12, 18, 24). The outputs are upsampled or downsampled with convolutional resizing adapters to match the dimensions of the corresponding multi-scale Learned Features Backbone outputs. Corresponding outputs from the two backbones are concatenated along the feature channel dimension.

The DINOv3-L variant was selected due to the high representation capacity of the model. However, in practical robotics applications, the model might be too large for deployment. Therefore, experiments were also carried out with smaller DINOv3-B and DINOv3-S models. For these models, hidden states (3, 6, 9, 12) were used as backbone outputs.

Squeeze-and-Excitation Channel Reduction (C) Concatenation of the outputs from the two backbones results in a high number of extracted features. To reduce the number of feature channels for the Segmentation Decoder, the SE Channel Reduction block was implemented. The detailed contents of the block are visualized in Fig. 2. The block follows a standard residual SE block architecture, with the exception that the feature channel is reduced in a stepwise fashion. The first convolutional layer in the block outputs a channel dimension of C_{mid} , which is defined as

$$C_{\text{mid}} = \max \left(\left\lfloor \frac{C_{\text{in}}}{2} \right\rfloor, C_{\text{out}} \right), \quad (1)$$

where C_{in} denotes the number of channels in the input, and C_{out} denotes the number of channels in the output. The stepwise channel reduction is implemented to avoid drastic reduction in channel dimension in just a single convolutional layer. Outputs are formatted to the same dimensions as the Swin-S outputs, to enable convenient integration of the dual-backbone into existing segmentation architectures.

The SE operation is added to the channel reduction to provide an attention-mechanism, which allows the network to identify and focus on relevant features.

Information in the feature channels of the general visual features and its derivatives can have varying levels of importance for the task. The SE block enables amplification and dampening of specific feature channels, respectively.

Segmentation Decoder (D) A standard Mask2Former Decoder was adopted to generate segmentation masks from the extracted feature representations. The decoder consists of a pixel decoder and a transformer decoder. The pixel decoder employs a deformable attention transformer [28] to fuse multi-scale features and produce dense, high-resolution pixel embeddings. The transformer decoder leverages global context through attention mechanisms to generate mask predictions based on the pixel decoder outputs, in a DETR-style query formulation [1]. The transformer decoder and pixel decoder outputs are combined, and the final binary segmentation mask is derived based on the query masks.

The standard decoder design choice results in most of the representational capacity of the architecture being in the dual-backbone, keeping the decoder lightweight. The decoder model is configured for a Swin-S backbone, with the dual-backbone and SE Channel Reduction providing features of the same dimensions as the standalone Swin-S outputs.

4 Experiments

4.1 Datasets

Four datasets were utilized to assess the performance of the proposed L+GNet. Datasets were selected based on wide representation in previous literature [10, 18, 26]. The datasets used were GDD [16], Trans10k-Stuff [25], GSD [12], and HSO [26]. L+GNet and its variants were trained on the respective training splits and evaluated on the corresponding testing splits. Additionally, an experiment was conducted where the model was trained on all of the available training splits combined, and evaluated on the testing splits. GDD features 2980 training images, and 936 images for testing. Trans10k-Stuff is a subset of the Trans10k dataset, consisting of only images which solely contain masks for the “Stuff” category of the dataset, referring to glass surfaces. The subset has a total of 2455 training images, and 1771 testing images. The GSD dataset depicts glass surfaces in a wide variety of environments, including residential apartments, public spaces, as well as outdoor areas. GSD contains 3285 images for training, and 813 images for testing. HSO is a recently published dataset for glass segmentation, focusing on glass surfaces in residential scenes. The dataset contains 3070 images for training and 1782 images for testing.

4.2 Implementation details

L+GNet and its variants were implemented with PyTorch and Huggingface, with pretrained models acquired from Huggingface repositories. For Mask2Former Decoder and Swin-S, ADE20k pretrained weights were used for initialization.

Hyperparameters for the Mask2Former Decoder and Swin-S were taken directly from the Huggingface implementation. A reduction ratio of 8 was used in the SE blocks of the architecture. Loss function from the original Mask2Former paper [2] was used for training the models.

In all experiments, L+GNet and its variants were trained for 30 epochs with a batch size of 16, using the AdamW optimizer, with a weight decay of 10^{-4} . A linearly decreasing learning rate scheduler was used, with an initial learning rate of 10^{-4} , and a warm-up of 500 steps. PyTorch mixed precision was used during training to reduce the memory footprint. During training, random horizontal and vertical flips were used for data augmentation. During training and testing, images were resized to 512×512 pixels prior to being fed to the models. All accuracy testing was carried out with FP32 precision. Inference speeds were tested with both FP16 and FP32 precision, using an RTX3090 graphics card for running the models.

Following recent literature [10, 18], four metrics were used for evaluating model performance: intersection-over-union (IoU), F-measure (F_β) with $\beta^2 = 0.3$, mean absolute error (MAE) and balanced error rate (BER). MAE results reported for our models have been computed with binary confidences. This was due to the DETR-style Mask2Former segmentation decoder struggling to provide calibrated confidence values, as highlighted in the presented results.

4.3 Accuracy Benchmark

Results for the accuracy benchmark on the four datasets are shown in Table 1, with comparison to scores achieved by other methods available in the literature. Additionally, Table 2 compares the performance of L+GNet with the previous state of the art when trained on the combined training data of all four datasets. The proposed L+GNet achieved the best IoU, MAE, and BER scores, on all the datasets. Highest F_β scores were achieved on all datasets except HSO, on which GlassWizard reached a slightly higher score. Overall, the results show that L+GNet has the capability to perform well on a high number of datasets, improving state-of-the-art results by a notable margin on most metrics. Samples of segmentation masks produced by L+GNet on the testing sets are visualized in Fig. 3. Failure cases of L+GNet segmentation results are shown in Fig. 4. Also, a visual comparison to previous state of the art is shown in Fig. 5, highlighting challenging scenarios where previous state of the art fails, yet L+GNet manages to perform segmentation well.

Although L+GNet excels in binary segmentation, it was noted that the model had difficulties providing calibrated prediction confidences. Calibration curves (i.e. reliability diagrams) for each dataset are presented in Fig. 6. The model was rarely reporting confidence values at either extreme of the scale, with few predictions assigned confidence values outside of an interval of approximately 0.3 to 0.7.

Table 1: Segmentation accuracy benchmark of different models on multiple datasets. Models trained and tested separately on respective datasets. Results for SAM [5], GlassSemNet [13] and C-LPMoE [21] taken from the respective papers. Results for VBNet, EBLNet and GDNet-B taken from [18]. Results for GlassWizard taken from the supplementary material of the paper [10]. Results for GDNet [16] and GSDNet [12] taken from respective papers as well as from [26]. Other benchmark results taken from [26]. Bolded values indicate the best result in each column. Colored percentage values indicate the relative difference of L+GNet results compared to best results in the previous literature.

Model	GDD [16]				GSD [12]			
	IoU \uparrow	F_{β} \uparrow	MAE \downarrow	BER \downarrow	IoU \uparrow	F_{β} \uparrow	MAE \downarrow	BER \downarrow
SAM [5]	0.485	0.798	0.268	26.08	0.506	0.799	0.213	23.91
TransLab [25]	0.816	-	0.097	9.70	0.781	-	0.069	9.19
Trans2Seg [23]	0.844	-	0.078	7.36	0.797	-	0.069	8.21
GDNet [16]	0.876	0.937	0.063	5.62	0.825	-	0.058	6.41
GSDNet [12]	0.875	0.932	0.059	5.71	0.836	0.903	0.055	6.12
EBLNet [6]	0.882	0.935	0.056	5.38	0.817	0.878	0.059	6.75
PGSNet [26]	0.878	-	0.062	5.56	0.836	-	0.054	6.25
GDNet-B [17]	0.878	0.939	0.061	5.52	-	-	-	-
GlassSemNet [13]	0.908	0.950	0.045	4.34	0.856	0.920	0.044	5.60
VBNet [18]	0.907	0.948	0.048	4.70	0.861	0.921	0.043	5.51
C-LPMoE-u [21]	0.923	-	0.039	-	-	-	-	-
GlassWizard [10]	0.921	0.961	0.041	3.86	0.891	0.942	0.035	4.14
L+GNet	0.948	0.972	0.025 ¹	2.50	0.931	0.961	0.024 ¹	2.54
	+2.7%	+1.1%	-36%	-35%	+4.5%	+2.0%	-31%	-39%
Model	Trans10K-Stuff [25]				HSO [26]			
	IoU \uparrow	F_{β} \uparrow	MAE \downarrow	BER \downarrow	IoU \uparrow	F_{β} \uparrow	MAE \downarrow	BER \downarrow
TransLab [25]	0.871	-	0.051	5.44	0.743	-	0.123	12.00
Trans2Seg [23]	0.750	-	0.124	10.73	0.780	-	0.095	9.65
GDNet [16]	0.887	-	0.046	4.72	0.787	-	0.097	9.32
GSDNet [12]	0.897	-	0.042	4.52	0.789	-	0.103	9.79
PGSNet [26]	0.898	-	0.042	4.39	0.801	-	0.089	9.08
VBNet [18]	0.916	0.955	0.032	3.41	0.831	0.900	0.078	7.65
GlassWizard [10]	0.930	0.965	0.028	2.91	0.867	0.929	0.062	6.06
L+GNet	0.947	0.972	0.022 ¹	2.24	0.881	0.928	0.045 ¹	4.50
	+1.8%	+0.7%	-21%	-23%	+1.6%	-0.1%	-30%	-26%

¹ With binary prediction confidences.

Table 2: Segmentation accuracy comparison to previous state of the art, with models trained on all of the datasets. Results for GlassWizard taken from the respective paper [10]. Bolded values indicate the best result in each column. Colored percentage values indicate the relative difference of L+GNet results compared to previous state of the art.

Model	GDD [16]				GSD [12]			
	IoU \uparrow	F_{β} \uparrow	MAE \downarrow	BER \downarrow	IoU \uparrow	F_{β} \uparrow	MAE \downarrow	BER \downarrow
GlassWizard [10]	0.933	0.969	0.039	3.62	0.904	0.952	0.036	4.03
L+GNet	0.951	0.974	0.023 ¹	2.33	0.938	0.965	0.022 ¹	2.28
	+1.9%	+0.5%	-41%	-36%	+3.8%	+1.4%	-39%	-43%
Model	Trans10K-Stuff [25]				HSO [26]			
	IoU \uparrow	F_{β} \uparrow	MAE \downarrow	BER \downarrow	IoU \uparrow	F_{β} \uparrow	MAE \downarrow	BER \downarrow
GlassWizard [10]	0.928	0.965	0.030	3.04	0.879	0.941	0.055	5.44
L+GNet	0.951	0.973	0.020 ¹	2.05	0.893	0.934	0.040 ¹	3.98
	+2.5%	+0.8%	-33%	-33%	+1.6%	-0.7%	-27%	-27%

¹ With binary prediction confidences.



Fig. 3: Samples of segmentation masks produced by L+GNet on the different testing sets. Model trained with the combined training sets. True positives overlaid in green, false positives overlaid in red, and false negatives overlaid in blue.



Fig. 4: Visualizations of failure cases encountered with the L+GNet model. Model trained with the combined training data. True positives overlaid in green, false positives overlaid in red, and false negatives overlaid in blue.



Fig. 5: Visualizations of L+GNet performance for images that the previous state of the art fails to correctly segment. L+GNet model trained with combined training data. GlassWizard results provided by the respective authors [10]. True positives overlaid in green, false positives overlaid in red, and false negatives overlaid in blue.

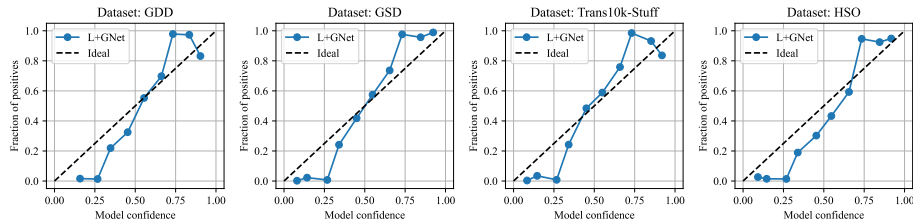


Fig. 6: Calibration curves for the L+GNet model on the datasets used for testing. Model trained on the respective training splits.

4.4 Ablation Study

Different ablations of the proposed architecture were tested, to quantify the impact of different design choices on the performance of the model. Results for the ablation study are presented in Table 3. Mask2Former w/ Swin-S represents exclusion of the General Features Backbone, whereas Mask2Former w/ DINOv3-L represents exclusion of the Learned Features Backbone. Acquired results highlight the performance gains of the dual-backbone. As the L+GNet architecture by default uses the DINOv3-L models, smaller versions of the DINOv3 backbone were also tested. L+GNet w/ DINOv3-B represents tests with the base-model, and L+GNet w/ DINOv3-S represents tests with the small-model. Results highlight that using the base-model in the backbone maintains high accuracy in the predictions, whereas the usage of the small-model significantly hinders performance. Also, an ablation of the L+GNet architecture without the SE Channel Reduction was included (L+GNet w/o SE), replacing the blocks with simple 1×1

convolutions. The results showed notable drops in performance on the GDD and GSD datasets, while nearly identical results were acquired on the Trans10K-Stuff and HSO datasets.

Table 3: Ablation study of the proposed method. Models trained and tested respectively on each dataset. Mask2Former w/ Swin-S and Mask2Former w/ DINOv3-L show single backbone solutions. L+GNet w/ DINOv3-B and L+GNet w/ DINOv3-S show smaller DINO variants in the General Features Backbone. L+GNet w/o SE shows removal of the SE Channel Reduction blocks. Bolded values show the best results in each column.

Model	GDD [16]				GSD [12]			
	IoU \uparrow	F_{β} \uparrow	MAE \downarrow ¹	BER \downarrow	IoU \uparrow	F_{β} \uparrow	MAE \downarrow ¹	BER \downarrow
Mask2Former w/ Swin-S	0.916	0.955	0.041	4.10	0.891	0.939	0.039	4.21
Mask2Former w/ DINOv3-L	0.928	0.965	0.034	3.48	0.918	0.955	0.029	3.13
L+GNet w/ DINOv3-B	0.933	0.962	0.033	3.22	0.922	0.955	0.028	2.90
L+GNet w/ DINOv3-S	0.918	0.956	0.040	3.96	0.896	0.943	0.037	4.08
L+GNet w/o SE	0.939	0.968	0.029	2.93	0.918	0.955	0.029	3.10
L+GNet	0.948	0.972	0.025	2.50	0.931	0.961	0.024	2.54

Model	Trans10K-Stuff [25]				HSO [26]			
	IoU \uparrow	F_{β} \uparrow	MAE \downarrow ¹	BER \downarrow	IoU \uparrow	F_{β} \uparrow	MAE \downarrow ¹	BER \downarrow
Mask2Former w/ Swin-S	0.932	0.963	0.028	2.88	0.828	0.894	0.067	6.79
Mask2Former w/ DINOv3-L	0.928	0.960	0.030	3.03	0.860	0.912	0.053	5.24
L+GNet w/ DINOv3-B	0.940	0.968	0.025	2.58	0.860	0.914	0.053	5.38
L+GNet w/ DINOv3-S	0.934	0.966	0.027	2.84	0.841	0.905	0.061	6.28
L+GNet w/o SE	0.947	0.972	0.022	2.25	0.879	0.928	0.045	4.63
L+GNet	0.947	0.972	0.022	2.24	0.881	0.928	0.045	4.50

¹ With binary prediction confidences.

4.5 Model Sizes and Inference Speeds

As robotics applications often depend on online and on-board usage of the models with limited computational power, inference speed of L+GNet and its variants was tested. Inference speeds were tested with both FP16 and FP32 precisions. Available open-source codes of the other methods in the literature were used to analyze their inference speeds on the same setup. Model sizes were also collected and compared between the L+GNet variants and other models in the literature. Inference speeds and model sizes are reported in Table 4. Reported inference speed values were measured as an average of one thousand forward passes for each model.

The inference speed test results highlight that the L+GNet model can be run on an RTX 3090 GPU at 14.2 fps (frames per second) on FP16 precision and at 8.0 fps on FP32 precision. Previous state of the art model GlassWizard [10] has a slightly faster inference speed than the default L+GNet model. However, the smaller L+GNet variant with a DINOv3-B backbone achieves a faster inference speed than GlassWizard, while still providing more accurate segmentation results on most datasets.

Table 4: Model sizes and inference speeds on an RTX 3090 GPU.

Model	Params (10^6)	Trainable params (10^6)	Inference speed FP16 (fps)	Inference speed FP32 (fps)
GlassSemNet [13]	240	240	19.8	16.6
C-LPMoE-u [21]	327	23.4	. ²	0.69
GlassWizard ¹ [10]	950	866	16.9	8.2
Mask2Former w/ Swin-S	68.7	68.7	26.3	24.9
Mask2Former w/ DINOv3-L	324	19.9	27.7	13.0
L+GNet w/ DINOv3-B	206	119	18.5	13.4
L+GNet w/ DINOv3-S	117	94.7	21.2	18.6
L+GNet w/o SE	404	99.3	15.6	8.8
L+GNet	450	145	14.2	8.0

¹ Inference model setup. Text encoder excluded.² FP16 not supported by the implementation.

5 Discussion

As shown by the accuracy benchmarks shown in Table 1 the proposed L+GNet model achieved the highest accuracy on nearly all of the metrics used, setting new state of the art records on the datasets used. In terms of pixel level classification, measured by the MAE and BER metrics, the model reached the highest accuracy in all experiments. The model also reached highest overlap of segmentation masks with regard to the ground truths, as indicated by IoU. On the F_β metric, the L+GNet model reached the highest result on three of the four datasets, being just slightly surpassed by GlassWizard [10] on the HSO dataset. This is likely due to the F_β metric being used with the weight of $\beta^2 = 0.3$, following the practices in the previous literature. This choice emphasises precision over recall in the metric. GlassWizard likely benefits from this choice, as the other metrics essentially evaluate precision and recall equally.

As shown in Fig. 4, some specific cases remain difficult for RGB-based glass segmentation. When there are minimal direct visual clues of a glass surface, yet a suitable surrounding is visible, the model is essentially forced to guess whether a glass surface is present. The model sometimes also interprets the whole scene to be observed through a glass surface. Additionally, the model may struggle to determine whether objects are positioned in front of a glass surface or behind it. Tape, posters, and other flat materials on glass surfaces can also mislead the model.

Regarding the chosen metrics, some studies available in the literature use the weighted F-measure F_β^w proposed by Margolin et al. [15], whereas other papers use the traditional F-measure F_β . This has led to apparent confusion in the literature, as the same numeric values can be found reported under two different metrics in different papers [18, 26]. The values used in the benchmark of this paper have been gathered from the literature according to the best of the authors’ judgement based on the available information.

All MAE results acquired with the L+GNet architecture and the considered ablations have been reported with binary predictions. Typically, these values are computed with the confidences of the model predictions. However, the architecture did not provide properly calibrated confidence values, as evident from

the calibration curves presented in Fig. 6. This is likely due to the DETR-style query-based segmentation strategy of the Mask2Former Decoder, fusing several mask predictions into the final prediction. To acquire calibrated prediction confidences, well-known post-processing strategies could potentially be applied [4].

To further experiment with L+GNet capabilities, different models could be chosen for the Learned Features Backbone of the architecture, including larger Swin variants. A lightweight model was chosen, since the amount of available training data is limited. Similarly, the width or depth of the Segmentation Decoder could be expanded as an attempt to improve the performance.

Although L+GNet with DINOv3-L backbone scored highest results, practical on-board application of the model in robotics could be more convenient with DINOv3-B backbone. Using this backbone likely provides a more feasible accuracy-speed trade-off for many applications, as evident from the results reported in Tables 3 and 4. DINOv3-B scored nearly similar results in terms of accuracy, while being notably more lightweight in terms of model size and computational load. However, the computational overhead and size of the General Features Backbone might not limit the applicability of the L+GNet model in specific processing pipelines. General visual features can be applied for several perception tasks, and the features can be shared by multiple perception heads performing different tasks. In perception pipelines where different branches utilize common foundation model features, the general visual features are available at no added computational cost for individual tasks.

6 Conclusion

This work proposed a novel deep learning architecture, L+GNet, for glass segmentation from RGB images. The key novelty in the architecture is a dual-backbone approach, which fuses features produced by a task-specific Learned Features Backbone, and a foundation model-based General Features Backbone. Features acquired from the backbones are downsampled with SE Channel Reduction, and fed into a Mask2Former Decoder which produces the final segmentation masks. This proposed architecture was proven to produce state-of-the-art results by a number of experiments carried out on different datasets widely used in the previous literature. In addition to accuracy benchmarks, the inference speed of the model was also studied, and found to be similar to previous state-of-the-art. However, in practical use the computational load might be notably reduced with a more lightweight General Features Backbone variant or with integration to a perception pipeline built on top of a foundation model. Future development of the model could focus on improving the calibration of the model confidence predictions. Additionally, a wider variety of models could be experimented for the Learned Features Backbone, as well as the Segmentation Decoder of the architecture.

Acknowledgements

This work was partially funded by Nokia Foundation under grant number 20250107, the NSERC Discovery Grants Program, and the Canada CIFAR AI Chairs Program. We gratefully acknowledge the computational resources provided by Aalto Science-IT.

References

1. Carion, N., Massa, F., Synnaeve, G., Usunier, N., Kirillov, A., Zagoruyko, S.: End-to-end object detection with transformers. In: European conference on computer vision. pp. 213–229. Springer (2020)
2. Cheng, B., Misra, I., Schwing, A.G., Kirillov, A., Girdhar, R.: Masked-attention mask transformer for universal image segmentation. In: Proceedings of the IEEE/CVF conference on computer vision and pattern recognition. pp. 1290–1299 (2022)
3. Dosovitskiy, A.: An image is worth 16x16 words: Transformers for image recognition at scale. arXiv preprint arXiv:2010.11929 (2020)
4. Guo, C., Pleiss, G., Sun, Y., Weinberger, K.Q.: On calibration of modern neural networks. In: International conference on machine learning. pp. 1321–1330. PMLR (2017)
5. Han, D., Zhang, C., Qiao, Y., Qamar, M., Jung, Y., Lee, S., Bae, S.H., Hong, C.S.: Segment anything model (sam) meets glass: Mirror and transparent objects cannot be easily detected. arXiv preprint arXiv:2305.00278 (2023)
6. He, H., Li, X., Cheng, G., Shi, J., Tong, Y., Meng, G., Prinet, V., Weng, L.: Enhanced boundary learning for glass-like object segmentation. In: Proceedings of the IEEE/CVF international conference on computer vision. pp. 15859–15868 (2021)
7. He, K., Zhang, X., Ren, S., Sun, J.: Deep residual learning for image recognition. In: Proceedings of the IEEE conference on computer vision and pattern recognition. pp. 770–778 (2016)
8. Hu, J., Shen, L., Sun, G.: Squeeze-and-excitation networks. In: Proceedings of the IEEE conference on computer vision and pattern recognition. pp. 7132–7141 (2018)
9. Huo, D., Wang, J., Qian, Y., Yang, Y.H.: Glass segmentation with rgb-thermal image pairs. *IEEE Transactions on Image Processing* **32**, 1911–1926 (2023)
10. Li, W., Ye, T., Xiong, X., Bai, J., Tang, F., Song, W., Xing, Z., Ju, L., Li, G., Zhu, L.: Glasswizard: Harvesting diffusion priors for glass surface detection. In: Proceedings of the IEEE/CVF International Conference on Computer Vision. pp. 17848–17858 (2025)
11. Lin, H., Zhu, Z., Wang, T., Ioannou, A., Huang, Y.: Glass surface segmentation with an rgb-d camera via weighted feature fusion for service robots. In: 2025 6th International Conference on Computer Vision, Image and Deep Learning (CVIDL). pp. 517–524. IEEE (2025)
12. Lin, J., He, Z., Lau, R.W.: Rich context aggregation with reflection prior for glass surface detection. In: Proceedings of the IEEE/CVF conference on computer vision and pattern recognition. pp. 13415–13424 (2021)
13. Lin, J., Yeung, Y.H., Lau, R.: Exploiting semantic relations for glass surface detection. *Advances in Neural Information Processing Systems* **35**, 22490–22504 (2022)

14. Liu, Z., Lin, Y., Cao, Y., Hu, H., Wei, Y., Zhang, Z., Lin, S., Guo, B.: Swin transformer: Hierarchical vision transformer using shifted windows. In: Proceedings of the IEEE/CVF international conference on computer vision. pp. 10012–10022 (2021)
15. Margolin, R., Zelnik-Manor, L., Tal, A.: How to evaluate foreground maps? In: Proceedings of the IEEE conference on computer vision and pattern recognition. pp. 248–255 (2014)
16. Mei, H., Yang, X., Wang, Y., Liu, Y., He, S., Zhang, Q., Wei, X., Lau, R.W.: Don't hit me! glass detection in real-world scenes. In: Proceedings of the IEEE/CVF Conference on Computer Vision and Pattern Recognition. pp. 3687–3696 (2020)
17. Mei, H., Yang, X., Yu, L., Zhang, Q., Wei, X., Lau, R.W.: Large-field contextual feature learning for glass detection. *IEEE Transactions on Pattern Analysis and Machine Intelligence* **45**(3), 3329–3346 (2022)
18. Qi, F., Tan, X., Zhang, Z., Chen, M., Xie, Y., Ma, L.: Glass makes blurs: Learning the visual blurriness for glass surface detection. *IEEE Transactions on Industrial Informatics* **20**(4), 6631–6641 (2024)
19. Rombach, R., Blattmann, A., Lorenz, D., Esser, P., Ommer, B.: High-resolution image synthesis with latent diffusion models. In: Proceedings of the IEEE/CVF conference on computer vision and pattern recognition. pp. 10684–10695 (2022)
20. Siméoni, O., Vo, H.V., Seitzer, M., Baldassarre, F., Oquab, M., Jose, C., Khalidov, V., Szafraniec, M., Yi, S., Ramamonjisoa, M., et al.: Dinov3. arXiv preprint arXiv:2508.10104 (2025)
21. Sun, Y., Lian, J., Yang, J., Luo, L.: Controllable-lpmoe: Adapting to challenging object segmentation via dynamic local priors from mixture-of-experts. In: Proceedings of the IEEE/CVF International Conference on Computer Vision. pp. 22327–22337 (2025)
22. Woo, S., Park, J., Lee, J.Y., Kweon, I.S.: Cbam: Convolutional block attention module. In: Proceedings of the European conference on computer vision (ECCV). pp. 3–19 (2018)
23. Xie, E., Wang, W., Wang, W., Sun, P., Xu, H., Liang, D., Luo, P.: Segmenting transparent objects in the wild with transformer. In: Proceedings of the International Joint Conference on Artificial Intelligence (2021)
24. Xie, E., Wang, W., Yu, Z., Anandkumar, A., Alvarez, J.M., Luo, P.: Segformer: Simple and efficient design for semantic segmentation with transformers. *Advances in neural information processing systems* **34**, 12077–12090 (2021)
25. Xie, E., Wang, W., Wang, W., Ding, M., Shen, C., Luo, P.: Segmenting transparent objects in the wild. In: European conference on computer vision. pp. 696–711. Springer (2020)
26. Yu, L., Mei, H., Dong, W., Wei, Z., Zhu, L., Wang, Y., Yang, X.: Progressive glass segmentation. *IEEE Transactions on Image Processing* **31**, 2920–2933 (2022)
27. Zhao, X., Schwertfeger, S.: 3dref: 3d dataset and benchmark for reflection detection in rgb and lidar data. In: 2024 International Conference on 3D Vision (3DV). pp. 225–234. IEEE (2024)
28. Zhu, X., Su, W., Lu, L., Li, B., Wang, X., Dai, J.: Deformable detr: Deformable transformers for end-to-end object detection. arXiv preprint arXiv:2010.04159 (2020)